Variety in the Coupling of Mesoporphyrin IX to Apohorseradish Peroxidase C Studied by Energy Selected Fluorescence Excitation and Vibronic Hole Burning Spectroscopy

Levente Herenyi,*,† Artur Suisalu,‡ Koit Mauring,‡ Katalin Kis-Petik,† Judit Fidy,† and Jaak Kikas§

Institute of Biophysics, Semmelweis Medical University, P.O. Box 263, H1444 Budapest, Hungary, Institute of Physics, Riia 142, EE2400 Tartu, Estonia, and Department of Physics, University of Tartu, Tahe 4, EE2400 Tartu, Estonia

Received: February 17, 1998; In Final Form: April 27, 1998

The coupling between the heme and the surrounding protein in horseradish peroxidase was studied after substituting the iron protoheme by mesoporphyrin IX to produce a sample measurable by high-resolution fluorescence spectroscopy. The inner ring phototautomerization of mesoporphyrin was used to create a variety of prosthetic group configurations that were shown to be stable at cryogenic temperatures. Due to the properties of the heme crevice, some tautomeric states are characterized by distinct spectral bands. The original band of the tautomeric form stable at room temperature (B_1) and two of those produced by photobleaching (B_2, B_3) could be selectively studied by two techniques, i.e., energy selected fluorescence excitation and vibronic hole burning spectroscopy. The line narrowed spectra were similar in the cases of complexes B_2 and B_3, while both are different from that of B_1. From these spectra, four characteristic vibronic lines were selected and further studied by spectral hole burning experiments. The unusual shapes of some spectral holes were discussed and interpreted on the basis of a new approach to the principles of energy selected spectroscopy. Vibronic relaxation times were determined and found in the range of 1−11 ps. It could be shown that in the porphyrin−protein complexes created photochemically at low temperature, some specific vibronic modes are characterized by significantly increased relaxation time values. It was thus experimentally verified that the coupling to the protein is the strongest in the lowest energy configuration stable at room temperature (B_1), in agreement with data of pressure tuning and of Stark effect hole burning studies on the same complexes.

Introduction

The fact that biochemically active molecules are found embedded in specific macromolecular matrices in biological systems points to the inherent importance of the coupling between the functional group and the surrounding macromolecular structure. Recent developments in the resolution of protein X-ray crystallography reveal that prosthetic groups in some hemoproteins[1] and in photosynthetic systems[2] acquire configurations that deviate from those in solutions and that are specific for the biological function. In the case of porphyrin type prosthetic groups, some of these characteristic distortions mean deviations from planarity that are achieved by interactions with the bulk protein and amino acid groups of the cavity. The purpose of these specific features in nature must be to achieve a certain biological activity. To understand the way in which structural properties are related to the regulation of biochemical processes is of basic importance. The properties relevant to biochemical reactivity could be revealed from the optical absorption and emission spectra of the functional group; however, the large inhomogeneous broadening makes it impossible to use the results of regular spectroscopic measurements for the interpretation of these fine effects. Energy selected spectroscopy, i.e., fluorescence line narrowing (FLN) and spectral hole burning (SHB), are high-resolution methods capable of monitoring the environmental effects free of inhomogeneous broadening. It has been shown previously that these methods can be successfully used to study the effect of the surrounding matrix also in the case of proteins.[3−6] The techniques applied for prosthetic groups embedded in proteins revealed irregular properties in the coupling of the chromophore and matrix.[7] As these properties are of biological significance and could be used in biotechnology, the FLN and SHB techniques are especially promising in these fields of study.

In the present work we have been studying the monomeric hemoprotein, horseradish peroxidase (HRP). The crystal structure of recombinant HRP isoenzyme C, published recently,[8] reveals also a distorted heme structure. To be able to use fluorescence methods, the native heme group—which is nonfluorescent due to the efficient nonradiative decay of the excited state—has been replaced by free base mesoporphyrin (MP). It has been shown earlier that the native structure important with respect to the coupling of the heme to the protein is only slightly affected by the substitution.[9] The MP substitution was not only a good technical solution for applying the FLN and SHB techniques, but the presence of a free base porphyrin in the protein made it possible to use the phototautomerization reaction of MP as a new and interesting tool in monitoring the interaction between an embedded porphyrin and the protein.[10,11] The phototautomerization of free base porphyrins is a well-known phenomenon characterized by the switching between the two linear and orthogonal positions of the two inner ring pyrrole hydrogens in the course of relaxation of the excited state. This

* Corresponding author.
† Semmelweis Medical University.
‡ Institute of Physics.
§ University of Tartu.

S1089-5647(98)01176-6 CCC: $15.00
Published on Web 07/01/1998

reaction is of high quantum yield and forms the basis of photochemical hole burning in free base porphyrins embedded in crystalline, e.g., in Shpolskii matrices. In the case of different crystal fields for the two linear tautomers, spectrally distinct origin bands are separated.[12] It has been shown, however, that, in proteins, more than two tautomeric forms characterized by distinct origin bands can be stabilized by the matrix.[13,14] Earlier spectral hole burning studies have shown that in MP−HRP four spectral bands can be observed that represent at least five distinct tautomeric configurations of MP−HRP complexes. These forms are separated by distinct energy barrier distributions in the ground state, demonstrating distinct protein compressibilities and porphyrin dipole properties as induced by the protein. It was especially a very interesting result that these distinct physical properties also arise when the complexes are formed photochemically at cryogenic temperatures from one single configuration that is stable at room temperature. This proved that a strict correlation exists between a prosthetic group configuration and protein conformation even at low temperature.[10,15]

In this work we have been applying the methods of FLN and vibronic SHB (VHB) to investigate the structural features of the MP forms coupled to HRP. Three different MP−HRP tautomeric complexes have been studied: two forms generated photochemically at low temperature are compared with the form stable at room temperature. The excitation FLN spectra of the three MP configurations are different: the excited-state vibrational profiles show some similarities between the two photoproduct species, while both have structural features distinct from the educt. VHB studies have been performed in four ranges of the FLN spectra of the three complexes. The spectral holes were analyzed and the hole width values were determined by Lorentzian fittings after the specific features arising from the technique of VHB had been interpreted. The vibronic relaxation times were longer in the case of the photoproduct complexes than that of the educt complex. This is an indication of having a stronger coupling in the structure that corresponds to the energy minimum configuration in the ground state of the porphyrin. The results show good agreement with structural predictions on the basis of temperature and pressure dependent SHB and Stark effect experiments on the same system.

Experimental Section

The native iron protoheme of HRP was replaced by MP. HRP isoenzyme C2 was isolated from horseradish roots and purified as described by Paul and Stigbrand.[16] The pure fraction was treated with 2-butanone,[17] and the apoprotein was recombined with purified MP IX from Porphyrin Products (Logan, UT) dissolved in ethanol. Samples were prepared and stored in 50 mM ammonium acetate, pH 5 at 200 K. The pH of the samples was adjusted to pH 8 by dialysis. To ensure transparency, glycerol was added to make a 50% (v/v) solution; thus the final concentration of MP-HRP was 20 μM.

Fluorescence excitation spectra and spectral hole burning experiments were carried out by a spectrometer setup consisting of a Coherent CR-490 tunable linear dye laser (bandwidth $\approx$ 0.5 cm^{-1}) with Rhodamine (6G) 590 (Exciton Co.) pumped by an argon ion laser (Coherent Innova 70-4)[18] and of a double grating monochromator (Lomo DFS-24, linear dispersion of 0.45 nm/mm). The dye laser output power was stabilized over the whole region of dye lasing (568−625 nm, 17 605−16 000 cm^{-1}), and its power density at the sample was kept in the range of 0.1−10 mW/cm^2. Neon emission lines were used as markers (by optogalvanic effect) for an exact determination of frequencies (calibration of frequency scale). The fluorescence signal was recorded by an RCA 31034 photomultiplier in photon counting mode and accumulated in a multichannel analyzer (Nokia LP4900B). Spectra were recorded by scanning the laser frequency over the inhomogeneous bands of interest and detecting fluorescence either in a broad-band mode, through a cutoff filter at wavelengths > 625 nm, or in an energy selected mode, when the emission was registered through the monochromator. The light source for selective photobleaching was the same laser as in the spectrometer setup; in the case of nonselective irradiation, a KGM-70 incandescent lamp (white light) has been used.

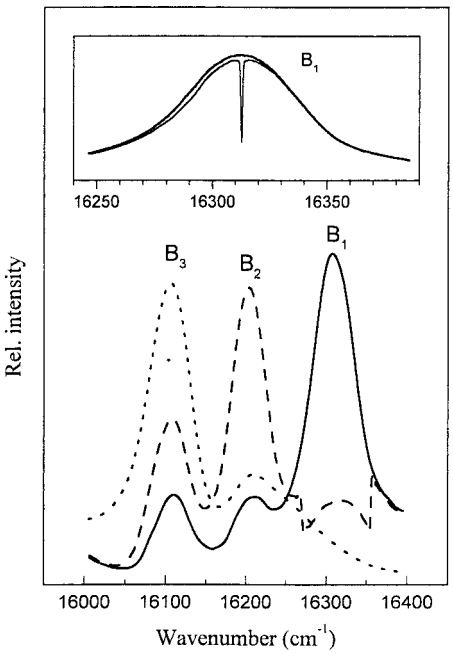

Figure 1. Fluorescence excitation spectra of MP−HRP in the Q_x region at 5 K, exhibiting different tautomeric bands due to irradiation at low temperature (the respective bands of the tautomeric states are labeled B_1 to B_3): the spectrum before irradiation (solid line), after selective photobleaching of B_1 band (dashed line), and after nonselective irradiation by white light (dotted line). The wavenumber range of the selective bleaching is clearly seen by the sharp edges of the spectrum in B_1 band (16 270−16 356 cm^{-1}). Inset shows the B_1 band with a deep laser-limited hole for determining the exact bandwidth of the dye laser.

Holes were burnt in the vibronic bands with the tunable dye laser. Burning power densities were 5−200 mW/cm^2, and the burning times varied between 20 and 200 s. The holes were subsequently probed by scanning the excitation spectrum with the same laser at reduced intensity (at about 1% of the burning intensity) and detected through the monochromator in the 0−0 range with a rather wide recording slit width (see Discussion). For determining the exact bandwidth of the dye laser, a deep laser-limited hole was also burnt in the 0−0 band and fitted by a Lorentzian.

All spectral measurements have been done at 5 K by using a temperature controlled (via vapor flow rate) He immersion cryostate.

Results

Energy Selected Excitation Spectroscopy. Figure 1 shows the fluorescence excitation spectra of the main tautomeric bands of MP−HRP in the Q_x region at 5 K. For convenience we have labeled the respective bands in an arbitrary fashion by B_1 to B_3 as it was done in previous papers.[10,19] The solid line shows

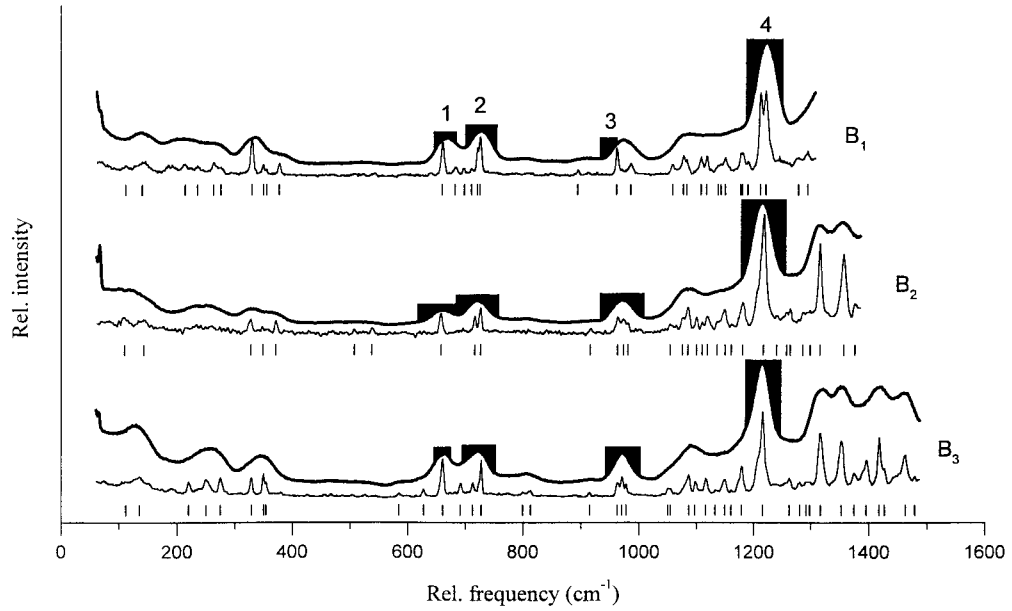

Figure 2. Energy selected excitation spectra of MP−HRP at 5 K in different tautomeric bands on a relative frequency scale (difference of excitation frequency and recording frequency, $\nu_{exc} - \nu_{rec}$). The recording frequencies are 16 309, 16 202, and 16 100 cm^{-1} for states B_1, B_2, and B_3, respectively. Thick lines represent a broader-band detection (of 26 ± 0.6 cm^{-1} spectral width); thin lines represent a narrower-band detection (FLN) (of 2.3 ± 0.05 cm^{-1} spectral width). Dominant spectral lines are labeled by markers below the spectra; respective frequencies are given in Table 1. Scanned frequency ranges for vibronic hole burning are marked by dark shaded areas and numbering.

the original spectrum after cooling to 5 K. The dashed line shows the spectrum after selective photobleaching of the B_1 band; a dominant band, B_2, appears. The wavenumber range of the selective bleaching is clearly seen by the sharp edges of the spectrum in the B_1 band (16 270−16 356 cm^{-1}). The dotted line shows the spectrum after nonselective irradiation by white light. In this case, the intensity of band B_3 is increased strongly with respect to B_2. The overall intensities are the same for all three spectra,[11] which means that the intensity change of the bands is due only to the population of the respective states.

The inset in Figure 1 shows the B_1 band with a deep laser-limited hole. In this way the exact bandwidth of the dye laser can be determined. This hole was fitted by a Lorentzian and the laser bandwidth was estimated by half of its full width at half-maximum (fwhm) ($\Gamma_{laser} = \Gamma_{hole}/2$) as $\Gamma_{laser} = 0.4$ cm^{-1}.

In Figure 2, the energy selected excitation spectra of the MP−HRP tautomer complexes are shown at 5 K. The fluorescence was registered selectively in the maxima of the corresponding tautomeric bands (for B_1 at 16 309 cm^{-1}, for B_2 at 16 202 cm^{-1}, and for B_3 at 16 100 cm^{-1}). Selectivity is determined by the slit width of the monochromator. The spectra are plotted on a relative frequency scale, which means the difference of excitation frequency and recording frequency ($\nu_{exc} - \nu_{rec}$). The scanned frequency range is thus limited by the emission of laser dye (upper limit) and the recording frequency (lower limit). Thick lines represent a broader-band detection with a slit width of 2.2 mm, corresponding to 26 ± 0.6 cm^{-1} resolution in this frequency range, thin lines represent a narrower-band detection (FLN) with a slit width of 0.2 mm, corresponding to 2.3 ± 0.05 cm^{-1} resolution. In both cases, the accuracy is better than 1 cm^{-1}. The dominant spectral lines are labeled by markers below the spectra, and the respective frequencies are given in Table 1.

The spectra of broader-band detection do not show significant peculiarities, but in the FLN spectra, differences between the tautomeric complexes can be observed. The overall features show some similarities in case of complexes B_2 and B_3, while both are different from B_1 (see for example the spectra around 950 and 1200 cm^{-1}). This figure also shows the frequency ranges where the scanning in the VHB experiment has been performed. These are marked by dark shaded areas and numbered for further references.

Vibronic Hole Burning Spectroscopy. Four vibronic holes were burnt for detailed analysis in each tautomeric spectrum nearly at the same spectral lines or line groups. In the case of VHB experiments, it can be expected that the holes will be rather broad. Thus their detection should be performed by a wide slit of the monochromator not to distort the shape of the holes (see Discussion). For avoiding another source of artificial distortions, before tuning the laser to the next vibronic line for burning, the previous hole was filled by thermal restoration or by white light irradiation.

In Figure 3 typical vibronic hole profiles are presented. We divided the holes into three groups: Figure 3a represents an ordinary, so-called single-line hole, in Figure 3b a double-line hole, and in Figure 3c a multiline hole are shown. These names reflect the shape of the spectra in the vicinity of the burning frequency. Insets show a broader spectral range of the excitation FLN spectra near the holes on the same relative frequency scale ($\nu_{exc} - \nu_{rec}$) as in Figure 2, and arrows mark the burning frequencies. It will be shown in the Discussion that the special features of the holes arise from the line structure of excitation FLN spectra and from the wide slit detection of the emission necessary for the technique.

Figure 4 represents an example of experimental results for determining the homogeneous vibronic holewidth (δ) in the case of a single-line hole. More complicated cases will be discussed in the next section. At least three holes have been burnt at the same frequency with the same intensity but increasing burning time (20 s, 40 s, 80 s) as shown in Figure 4a. The holes were fitted by Lorentzians. The evaluation has been performed by two different kinds of baseline corrections. The fwhm was plotted as a function of burning time in Figure 4b for the two series. The data were fitted by a straight line and a linear extrapolation for $t \rightarrow 0$ yielded the δ that had been used for determining the homogeneous line width (Γ) of vibronic

TABLE 1: Comparison of Vibrational Frequencies ($\nu_{exc} - \nu_{rec}$, cm^{-1}) in the First Excited Singlet State of Different Tautomeric Forms of MP−HRP (See Spectra in Figure 2), of MP−HRP at pH 5 (B_3*), of Metal-free Myoglobin (Mb), and of Porphine in the Xe Matrix (Xe)[a]

B_1	B_2	B_3	B_3*	Mb	Xe	B_1	B_2	B_3	B_3*	Mb	Xe
112 wbr	110 br	112 wbr			108 w	985				988	985
140 br	143 br	135 br		137 w	152					994	990
214 w		220	223						1038	1045 w	
235 w				244				1051 w	1051	1051 w	1049 s
		250		260 br		1058 w	1054 w	1055 w	1060		
263				265 br		1076	1076				
276 w		275				1083	1085	1087	1080	1083	
				291	304 s		1100	1098	1095	1100	1105
				318 br		1107	1109 w			1109	
330 s	328	329		324 br		1117	1119	1116	1115		
350	349 w	350		351		1137 w	1136 w	1133 w		1130	
355 w		354				1142 w			1145	1140	
377	371			370		1150	1150	1150			
				388			1160 w	1160 w		1168	1159 s
				396		1176					
				422	411 w	1180	1181	11790 s	1178		
				452	456 w	1189 w				1198	
				475 w		*1211 vs*			1210		1211 s
				485 w			*1217 vs*	*1216 vs*		1217	
	507 w			503 w		*1221 vs*					
	537 w			532 w			1240 w		1236	1245 w	
		585 w		592 w			1257		1258		
					610 w		1264	1262			
		628		640		1278 w	1285 w	1281 w	1271	1272	
659 s	*657 s*	*661 s*		656		1294		1292 w	1290		1292 s
				674			1298 w	1298 w		1298	1301 s
681 w				681			1315 vs	1317 vs	1312	1320	1311 s
698 w		692		702 w					1324		1324 s
710 w					710 s						1329 s
720 s	*716 s*	713								1339	1333 s
725 s	*726 s*	*728 s*	724	723	728 w				1348		1347 s
			760	750 w			1357 vs	1353 vs		1358	1359 s
				764					1367		
					781		1376	1375		1376 w	
		800 w		796 w				1395 s		1390	1390
		813 w	810	810 w						1406	1399
				820 w				1418 vs			1412 w
				860 w	861 w			1427		1438	
				880 w						1455	
893 w			883	890 w				1463 s			1464
	916 w	915 w	910	917 w				1479 w		1477	1478
			926	924							
				945 w	939 s						
961 s	*963*	*963*	960	960	965						
	973	*971*	968								
	981	*978*	976								

[a] Relative intensities of lines are marked with letters: w, weak; s, strong; vs, very strong. Italic numbers represent the frequencies of typical vibronational transitions where the vibronic hole burning experiment has been performed.

transition by the relation

$$\Gamma = \delta/2 - \Gamma_{laser} \quad (1)$$

where Γ_{laser} is the estimated laser bandwidth. The vibronic relaxation time was calculated by the formula $\tau = (2\pi\Gamma)^{-1}$. These parameters (δ, Γ, τ), the burning frequency (ν_{burn}), and the typical vibrational frequency of the transitions (ν) are given in Table 2 for all three MP−HRP tautomeric complexes (B_1, B_2, B_3) and for the four selected vibronic lines. The relaxation time values were within the 1−11 ps range. The phototautomerization that produced complexes B_2 and B_3, however, seemed to significantly increase the relaxation time of certain vibronic levels.

Discussion

Interpretation of Excitation FLN Spectra and Analysis of Vibronic Hole Shapes. The FLN spectra shown in Figure 2 have been measured by scanning the narrow-band laser excitation in the region of vibronic absorption and by detecting the emission through a narrow-slit monochromator at the maxima of the respective tautomeric origin bands (B_1, B_2, B_3). General discussion of the FLN technique has been given in numerous papers and reviews,[18,20,21] and, similarly, the VHB technique has been discussed and applied by several authors.[22−26] For interpretation of our experiments, however, a short overview of basic principles may be useful.

It is well-known that the conventional fluorescence excitation spectra of chromoproteins consist of broad bands even at low temperature due to the inhomogeneous environment of chromophore molecules. This broadening of spectral lines means that the differences of level energies obey statistical distributions. We adopt the simplest phenomenological model of inhomogeneous broadening, assuming that, for all the vibrational levels of a given electronic state, the energy differences

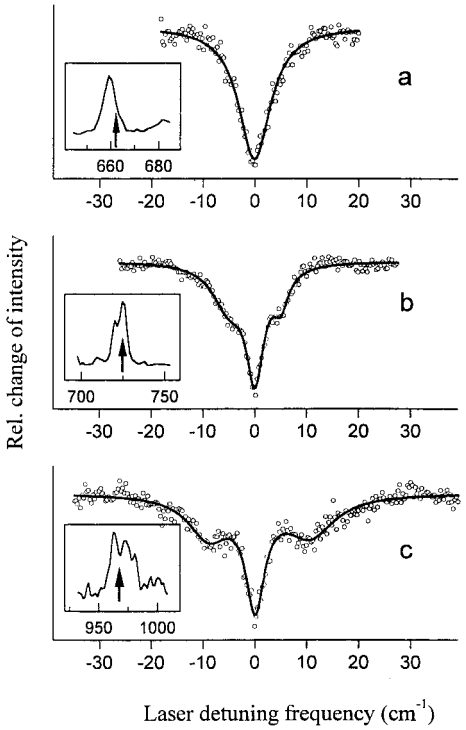

Figure 3. Typical shapes of vibronic holes: (a) single-line hole; (b) double-line hole; (c) multiline (more than two) hole. Insets show the local section of energy selected excitation spectra near the holes on the same relative frequency scale ($\nu_{exc} - \nu_{rec}$) as in Figure 2, and arrows mark the burning frequencies.

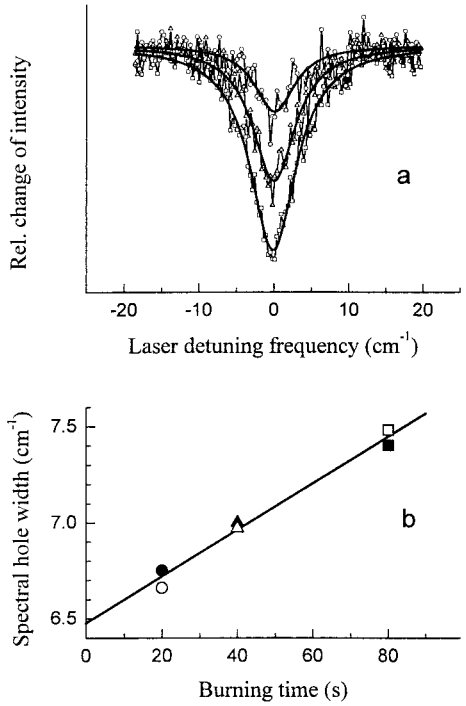

Figure 4. Evaluation of the homogeneous holewidth (δ). (a) Holes burnt at the same frequency with increasing burning time (shortest, open circles; medium, open triangles; longest, open squares) and at a constant intensity fitted to Lorentzians. (b) Holewidth as a function of burning time. Symbols correspond to the labeling of holes in a with the open−solid alternation indicating two different ways of baseline correction (see text).

$$\epsilon_{(0,q)} - \epsilon_{(0,p)} \quad \text{and} \quad \epsilon_{(1,s)} - \epsilon_{(1,r)} \text{ are constants} \qquad (2)$$

for all the chromophore molecules (one-dimensional inhomogeneity[22] or pure electronic distortion[27]). Here ϵ denotes the level energy and the indexes $(0,p)$ or $(0,q)$ and $(1,r)$ or $(1,s)$ (p, q, r, $s = 0$, l, 2, ...) label the vibronic levels in the ground and in the first excited electronic states, respectively. In this case, the inhomogeneous broadening can be described by the inhomogeneous distribution function (IDF), which may be mathematically given by a probability density function.

TABLE 2: Summary of the Vibronic Hole Burning Experiment[a]

site	hole no. and type	ν_{burn} (cm^{-1})	ν (cm^{-1})	δ (cm^{-1})	Γ (cm^{-1})	τ (ps)
B_1	1 (s)	663.5	659	6.5	2.9	1.8
	2 (d)	725.3	720 725	2.5	0.9	5.9
	3 (s)	948.3	961	4.2	1.7	3.1
	4 (m)	1216.9	1211 1221	10.0	4.6	1.2
B_2	1 (s)	665.5	657	4.0	1.6	3.3
	2 (d)	720.6	716 726	2.5	0.9	5.9
	3 (m)	974.1	963 973	3.7	1.5	3.6
	4 (m)	1214.9	981 1217	9.0	4.1	1.3
B_3	1 (s)	660.4	661	6.0	2.6	2.1
	2 (s)	723.0	728	3.1	1.2	4.4
	3 (m)	971.9	963 971	1.8	0.5	10.7
	4 (m)	1215.9	978 1216	6.0	2.6	2.1

[a] Sites correspond to different tautomeric forms; hole numbers are the same as those in Figure 2. Hole types: s, single line; d, double line; m, multiline (see Figure 3). Other symbols: ν_{burn}, burning frequency; ν, vibrational frequencies for the typical transitions; δ, homogeneous holewidth; Γ, homogeneous line width; τ, vibronic relaxation time.

Since in spectroscopy we measure the energy differences only, we may, for the sake of simplicity, assume that the spectral density functions (SDF) of chromophores for the ground-state levels are given by δ functions, i.e., $SDF_{(0,p)} = \delta(\epsilon - \epsilon_{(0,p)})$ ($p = 0, 1, 2, ...$), which means that all the chromophore molecules in a given ground-state vibrational level have the same energy. Then the SDFs for the first excited-state levels are given by simple shifts of a single IDF, which we denote by n in probability density function representation: $SDF_{(1,r)} = n(\epsilon - \langle\epsilon_{(1,r)}\rangle)$, where $\langle\epsilon_{(1,r)}\rangle$ is the expected value (mean) for the rth vibronic level energy in the excited state. It means that the IDF, n is characteristic for all the excited-state levels. Note that the assumptions in (2) represent a rather good approximation, and this is, in fact, the cornerstone for the success of the FLN spectroscopy. More careful considerations reveal, however, that even molecules with the same electronic gap may exhibit slightly different vibrational energies. We do not consider here the effects related to such higher-dimensional inhomogeneity.[26,28,29]

In an energy selected fluorescence experiment, the emission line intensity is given by the formula

$$I_{(r,p)} = KI_{exc}A_{(1,0)\rightarrow(0,p)}B_{(1,r)\leftarrow(0,0)}\Delta\epsilon_{exc}n(\epsilon_{exc} - \langle\epsilon_{(1,r)}\rangle) \qquad (3)$$

where $I_{(r,p)}$ is the line intensity of the $(1,0) \rightarrow (0,p)$ transition after an excitation of $(1,r) \leftarrow (0,0)$ and vibrational relaxation, K is a constant, I_{exc} is the excitation intensity, $A_{(1,0)\rightarrow(0,p)}$ is the fluorescence emission probability, $B_{(1,r)\leftarrow(0,0)}$ is the absorption transition probability, $\Delta\epsilon_{exc}$ is the bandwidth of laser excitation; $n(\epsilon_{exc} - \langle\epsilon_{(1,r)}\rangle)$ in the expression denotes the value of the respective SDF at the excitation energy of ϵ_{exc}.

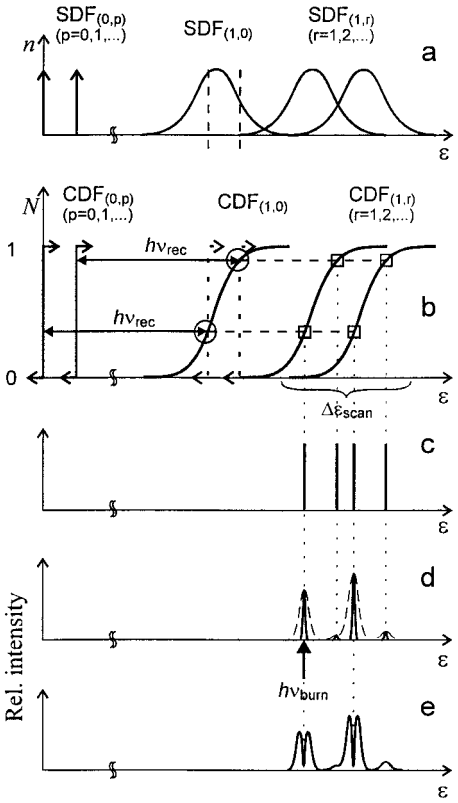

Figure 5. Interpretation of excitation FLN spectra and the origin of vibronic holes. (a) A set of overlapping spectral density functions (SDF) (using the IDF n). (b) The same set represented by cumulative distribution functions (CDF) (using the IDF N). The predefined $h\nu_{rec}$ "distance" along the energy scale shows the possible resonant transition for fluorescence emission. Circles mark the sites where fluorescence emission could happen from. The same sites of IDF are present in all the vibronic replica of $CDF_{(1,0)}$ ($CDF_{(1,r)}$, $r = 1, 2, ...$), which are marked with squares. The scanned energy range ($\Delta\epsilon_{scan}$) for laser excitation is also seen in this figure. (c) Positions of spectral lines marked with sticks. (d) A hypothetical excitation FLN spectrum (thick line) where we took into account that only the lines originating from the (0,0) transitions have well-detectable intensities (see text). Dashed line represents the same energy selected excitation spectrum with a wider slit detection (less selectivity). (e) Appearance of holes (also wider slit detection) after burning at the first intensive line ($h\nu_{burn}$) of the excitation FLN spectrum.

In graphic representations we found it very helpful to use the cumulative distribution functions (CDFs) instead of probability density functions to interpret the origin of the spectral lines in the excitation FLN technique. The advantage of this approach is that one can avoid the disturbing effect of overlapping broad SDFs in the schemes, and in this way the phenomena are easier to understand. Thus instead of n as above, we introduce N as CDFs according to the following relation:

$$P(\epsilon_1 < \epsilon < \epsilon_2) = \int_{\epsilon_1}^{\epsilon_2} n(\epsilon)\, d\epsilon = N(\epsilon_2) - N(\epsilon_1) \qquad (4)$$

where $P(\epsilon_1 < \epsilon < \epsilon_2)$ is the probability of finding a molecule with a level energy ϵ within the limits $\epsilon_1 < \epsilon < \epsilon_2$. These two kinds of representations of IDF can be seen in Figure 5a,b. The CDFs shown in Figure 5b are analogous with the energy level diagram representation suggested by Kaposi and Vanderkooi[30] that is a modified version of the Jablonski diagram. In this representation the vibronic energy levels form parallel curves, called vibronic "surfaces" by the authors. These surfaces are the inverse functions of the CDFs.

Consider the scheme in Figure 5, which shows a simple experimental condition for the application of the CDF concept. As was mentioned before, we assumed that the SDFs for the ground state levels are given by δ functions, consequently the CDFs for the same states ($CDF_{(0,p)}$, $p = 0, 1, 2, ...$) are given by step functions. Let us suppose that there is a sharp recording frequency (ν_{rec}) in the experiment. In Figure 5b, two ground-state $CDF_{(0,p)}$s with energy separation of $h\nu_{rec}$ from the first excited-state $CDF_{(1,0)}$ are shown. These emissions will be detected in the experiment. If the range of excitation has been chosen as shown in the figure by $\Delta\epsilon_{scan}$, four possible vibronic lines may become visible in the excitation FLN spectrum. These lines are shown in Figure 5c. The spectral resolution of the spectrum is limited by the slit width of the monochromator and the bandwidth of laser excitation. In practice, the former (slit) is usually wider than the latter; thus the monochromator determines the spectral resolution.

The intensities of the lines can be determined by eq 3. There are two important aspects. One has to choose the recording frequency in the middle of the SDF ($h\nu_{rec} = \langle\epsilon_{(1,0)}\rangle$) in order to get intense lines in (0,0) transition. Another effect arises from the fact that generally $A_{(1,0)\rightarrow(0,0)} > A_{(1,0)\rightarrow(0,p)}$ ($p = 1, 2, ...$). The outcome of these two effects is that only lines originating from the (0,0) transitions have well-detectable intensities (see Figure 5d). Thus, we can conclude that the spectral lines in the excitation FLN spectra, with a good approximation, correspond to the excited-state vibrational energy levels, and the lines which would originate from the presence of different ground-state vibrational energy levels practically do not appear in the spectra.

Note that in the case of wider slits, the lines will be broader. This effect is seen in Figure 5d (dashed lines) and also in Figure 2 as the difference between the spectra with thin and thick lines.

Hole Profiles. The interpretation of the multiple line feature in our VHB experiments can be based on the previous scheme (CDF), but it is more complicated, because we have to take into account the effect of the finite slit width.

Consider the hypothetical spectrum in Figure 5d and the case in which a subpopulation of molecules is removed by phototransformation at the frequency (energy) where the first intense line appears in the spectrum ($h\nu_{burn}$, marked by arrow). The consequence is that the product of $\Delta\epsilon_{exc}n(h\nu_{burn} - \langle\epsilon_{(1,r)}\rangle)$ and so the spectral line intensity drastically decreases according to eq 3. Since a well-defined subpopulation of molecules was affected, this effect occurs in all CDFs. Thus in Figure 5d not only the first but also the second line will disappear. If we scanned the same spectral range again by the excitation laser and monochromator of the same slit width, we would see nothing in place of the two intense spectral lines. If, however, one uses a much wider slit of the monochromator and repeats the scan, the unburnt parts of the spectrum (the surrounding parts of the previous narrow lines) will also appear, and one is able to detect the holes inside the broader lines (see Figure 5e). Thus by using too narrow slits of the monochromator one could overlook the hole or at least distort the hole shape.

In our experiments, we expected rather broad vibronic holes and our purpose was the determination of the homogeneous width of them; thus we had to use a very wide slit detection to avoid line distortions. This way of detection does not cause any problem if a single CDF can be separately measured, which means there is no other CDF in the range of detection. This case is shown in Figure 6a as $CDF_{(1,r)}$. When one burns a hole into this single band, a subpopulation of molecules (ΔN) will be removed; thus a series of satellite holes would also appear, but they are far from the burning frequency (or energy, $h\nu_{burn}$). So they will not be detected through the window which is

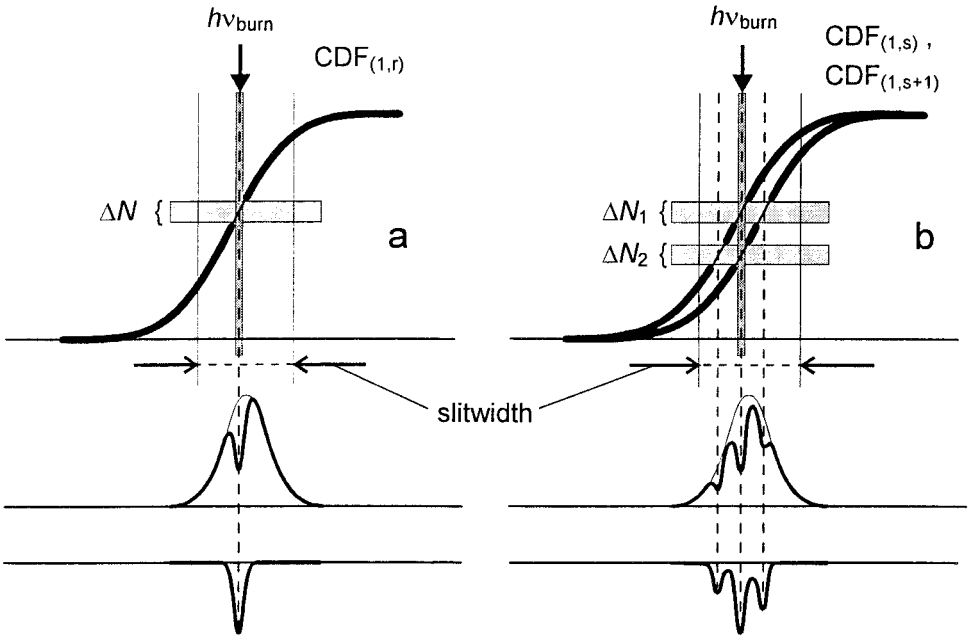

Figure 6. Simplified version of Figure 5, scheme for explanation of the complex hole shapes: (a) Single-line hole; (b) double-line hole. Upper part: IDF in CDF representation with the burning frequency (or energy, $h\nu_{burn}$) and the relative amount of burnt molecules (ΔN) (slit width is also represented). Middle part: Spectrum at a wider-slit detection (thin line, before; thick line, after burning). Lowest part: Hole profile.

determined by the slit width of the monochromator and the scanning range of laser excitation (single-line hole).

In the case in which two CDFs are close to each other (see in Figure 6b, $CDF_{(1,s)}$ and $CDF_{(1,s+1)}$), we cannot burn a single hole because at a certain burning frequency (or energy, $h\nu_{burn}$) a group of molecules (ΔN_1) will be removed via $CDF_{(1,s)}$ and another one (ΔN_2) via $CDF_{(1,s+1)}$. Nevertheless, the ΔN_1 subpopulation is also absent from $CDF_{(1,s+1)}$ and the ΔN_2 from $CDF_{(1,s)}$ (moreover ΔN_1 and ΔN_2 will be absent from all the CDFs). So we directly burnt two "main" holes at the same burning frequency simultaneously and a number of satellite holes, but only two of them appear symmetrically on both sides of the main holes rather close to the burning frequency. Since the above-mentioned window is wide enough, we will see these closest holes while all the other satellite holes are out of the detected range (double-line hole). (Note that in real cases the hole structure is never totally symmetrical because of the IDF and different transition probabilities.)

In the case of more than two closer CDFs, the situation is more complicated. The number of observable satellite holes inside the window further increases; thus the complex structure of them can be considered as background for the fitting (multiline hole).

Vibrational Modes of MP−HRP Tautomers and Their Connection with Vibronic Relaxation Results. Vibrational frequencies in the first excited singlet state of the three tautomeric forms of MP−HRP (B_1, B_2, B_3) are listed in Table 1, along with literature data of MP−HRP at pH 5 (B_3*),[31] those of metal-free myoglobin (Mb),[32] and of porphine in Xe matrix.[33] All the frequencies are given in wavenumbers, the corresponding lines with approximately identical frequencies are in one row. The correlation between two series (columns) can be characterized by the quotient of two parameters: the ratio of the number of matching lines to the total number of lines (R), and the mean of the frequency differences of paired lines, named as mean deviation (MD). Thus the higher the value of R/MD, the closer the correlation.

Comparison with Porphine in the Xe Matrix. The vibrational pattern of different tautomeric forms of MP−HRP are compared with porphine in Xe matrix. Porphine has two sites in the noble gas matrix with vibrational frequency differences up to 3 cm^{-1}. In this comparison we neglect these differences and compare with only one of these series (of site *A*). More than half of the porphine frequencies match within 8 cm^{-1} those of MP−HRP. Because of the substitutions on the porphyrin ring in MP and possible out-of-plane motions, clearly different vibrational frequencies may also be found, even if steric restrictions of the matrix are neglected (protein versus noble gas matrix). As an example, the lines around 330, 350, and 660 cm^{-1} of all the three tautomeric components of MP−HRP are not found in porphine, while specific porphine lines emerge at 610, 781, and 1329 cm^{-1}. The R/MD quotients for the tautomeric states (Xe−B_1, Xe−B_2, and Xe−B_3) are 0.1, 0.07, and 0.09, respectively. Despite the fewer lines in state B_1 (the measurement was limited by the laser dye emission) the correlation is the closest. The R/MD values calculated only for the frequency range, which is common for all three tautomers, are 0.1, 0.05, and 0.06. It means that state B_1 is probably the least distorted by the protein matrix.

Comparison with Metal-Free Mb. The energy selected excitation spectrum, which in turn gives the vibrational energies of the excited-state molecules, has been constructed from high-resolution emission spectra under energy selection conditions (FLN) of metal-free Mb.[32] It has been observed that, within the resolution of the technique, the vibrational frequencies of protoporphyrin (PP) in Mb are constant over the inhomogeneous distribution. This shows that the primary effect of the protein on the chromophore is to perturb the electronic energy levels through the electric field of the pocket, rather than to hold the porphyrin in a variety of defined strained configurations. However, this may not be a general result for all chromophores in proteins. For example in the case of MP in cytochrome *c* peroxidase most of the lines in the vibrationally resolved emission spectra remained constant over the IDF, but some excited-state vibrational modes shift with excitation frequency.[34] The significance of various strained forms of porphyrins in proteins has been emphasized in a review.[35]

The comparison of similar chromophores (MP and PP) in two different proteins, HRP and Mb, shows that their singlet excited-state vibrational frequencies differ by 4.5 cm^{-1} on the average. Some vibrational energies may differ because of the different substituent groups, but also the heme pockets of HRP and Mb may produce different steric restrictions for the individual tautomeric forms. In the low-frequency range of Table 1, more vibrational lines are observed in the case of metal-free Mb than in that of MP−HRP. Different steric conditions may affect both the Franck−Condon factors and the phonon coupling, which would account for such a difference.

The *R*/MD data in the whole and common frequency range for the three tautomeric states (Mb−B_1, Mb−B_2, and Mb−B_3) are 0.12, 0.16, 0.12 and 0.12, 0.13, 0.11, respectively; thus the closest correlation was found for the B_2 state.

Comparison of Different Tautomeric Forms of MP−HRP. FLN can sensitively detect differences in configurations of the porphyrin within the inhomogeneous distribution. Because the free-base mesoporphyrin has low symmetry, tautomerization may yield different vibrational frequencies. In addition, the asymmetrical heme pocket environment could produce additional differences in the tautomeric forms. In the earlier measurements[31] the vibrational frequencies could be determined only in a limited frequency range and only for the tautomer we now identified with band B_3. These data we will refer to as B_3*. (One has to remember that, in the earlier studies, the protein was at pH 5, while now, the pH was adjusted to 8.) From the available data the *R*/MD values were determined for the B_3*−B_1, B_3*−B_2, and B_3*−B_3, pairs. These are 0.16, 0.12, and 0.17, respectively. It is surprising that the correlation is not better than with the case of Mb. Nevertheless in an other earlier work[34] we found that at lower pH the protonated amino acids near the porphyrin influence the vibrational structure. The *R*/MD quotients for the present experiment show significantly better correlation: the values are 0.25 (B_1−B_2), 0.21 (B_1−B_3), and 0.33 (B_2−B_3). These data indicate the most pronounced similarity between complexes B_2 and B_3. These specialties were further studied by the VHB method.

Note that in the vibrationally resolved spectra some lines are quite narrow and symmetric, while others are broader and often seem to have shoulders. The reason for broadening may be the stronger coupling of certain vibronic states to phonons that lead to faster vibrational relaxation and increased homogeneous line width. Thus the coupling to the protein can indeed affect some vibrational modes more than others.[36] However the vibronic lines could also be inhomogeneously broadened, because selectivity of fluorescence detection does not remove the inhomogeneity of the vibrational energy due to the lack of correlation between electronic and vibrational energies. Finally, if there are two closely lying vibrational frequencies, the technique may not be able to resolve these. Indeed, the double line in state B_1 around 1215 cm^{-1} (1211−1221 cm^{-1}) seems to be single in states B_2 and B_3, but it has a definite shoulder, and in the most photostable (B_3) state it appeared to contain at least three components in a more detailed analysis.

Vibronic Hole Burning. The vibrational lines selected for VHB experiments were shown in Table 1 in italics and Table 2 together with characteristic parameters and also with the relaxation times. There are only a few literature data concerning comparable experiments. Sapozhnikov[37] after model calculations has studied the vibronic relaxation of coproporphyrin in a glassy ethanol matrix. He found that the vibrational relaxation time for the 725 cm^{-1} level in the excited electronic state of coproporphyrin is 1.5 ps. Avarmaa and Rebane[18] have measured pheophytin *a* and chlorophyll *a* in ether; the determined relaxation times were in the 1.1−6.6 ps range. They found that despite a higher complexity of the chlorophyll-type molecules, the vibrational relaxation is not notably faster than in the parent tetrapyrrole compounds.

Voelker and co-workers have measured porphine in crystalline *n*-alkanes in both crystallographic sites (*A* and *B*), having two tautomeric forms (1 and 2) in each site, and enlisted the determined excited-state vibrational energies and relaxation time values.[38,39] They found that the relaxation time strongly depends on guest−host coupling, on the nature of the site in which the molecule is incorporated, but did not find any correlation between the relaxation times and the vibrational energies. The relaxation time values in the less favored *B*-site were in the 5.7−122 ps range. In the thermodynamically more stable *A*-site they were in the 0.9−11 ps range, except of two extremely long relaxation times at 710 and 1161 cm^{-1} frequencies. This latter result is in good agreement with our data: the relaxation times were 1.2−10.7 ps (Sapozhnikov's and Avarmaa's results also fit into this range). The above-mentioned two lines were not detected in our system. The vibronic relaxation times of the tautomeric form 1 are generally shorter than those of form 2 in *n*-octane. This result is analogous to our finding in MP−HRP that the relaxation times are generally the shortest in the tautomeric complex stable at room temperature (B_1). The ratios of related relaxation times of the different tautomeric forms (e.g. $\tau\{\nu_i,1\}/\tau\{\nu_i,2\}$ or $\tau\{\nu_j,B_1\}/\tau\{\nu_j,B_2\}$) in the two systems are also similar. In case of porphine in *n*-octane they are between 1.1 and 0.5; in MP−HRP, between 1.3 and 0.3.

The identification of vibronic modes related to the spectral lines of some porphyrin derivatives have been performed on the basis of resonance Raman and FLN results.[40] We were able to relate vibrational energies of Table 2 to those. For hole 1, the typical vibrational frequency is around 659 cm^{-1} for all three tautomers. In octaethylporphyrin a similar frequency (658 cm^{-1}) has been ascribed to in-plane modes, but detailed identification of the modes has not been given unambiguously. The typical vibrational frequencies near hole 2 are in the range of 716−728 cm^{-1}. There are two reference lines at a frequency of 723 cm^{-1} for in-plane modes too. Deuterium substitution had only a slight effect on the frequencies of both vibrations, and the identification also suggests that both vibrations originate from the ring C−C and C−N modes. In the case of hole 3 a group of "typical" lines appears between 961 and 981 cm^{-1}. In the reference table the frequency of 976 cm^{-1} has been assigned to out-of-plane modes. Hole 4 can be characterized by a frequency range of 1211−1221 cm^{-1}. The original frequency in the reference table was 1226 cm^{-1} for out-of-plane modes, and the energy decreased upon deuterium substitution. In both latter cases the modes can be partially attributed to the N−H atoms of the porphyrin inner ring.

Conclusions

(1) Though we have only four data series of vibronic relaxation times in three cases of them (nos. 1, 3, 4), the respective values are shorter in tautomeric state B_1 than in the two others. On the basis of this observation it seems that as consequence of the formation of the phototautomeric complexes B_2 and B_3 at low temperature in the protein crevice, the process of vibronic relaxation slows down. This indicates that these tautomers (stable only at low temperature) have weaker interaction with the protein than tautomer B_1 (stable at room temperature too) has. This conclusion agrees with previously determined compressibility values that showed an increase from 0.11

GPa^{-1} for B_1 up to about 0.3 GPa^{-1} in the case of states B_2 and B_3.[10] This difference in the coupling was also shown in a Stark effect hole burning study. The $\Delta\mu_0$ difference between the permanent dipole moment in the ground and electronically excited state of the porphyrin, induced by the protein, was significantly different in state B_1, where $\Delta\mu_0 \approx 0$ as compared to states B_2 and B_3, where $\Delta\mu_0 \neq 0$.[15] As could be seen in Table 2, some vibrations are more sensitive to details of the guest−host coupling than others.

(2) As discussed above, the line near hole 2 in Table 2 can be identified as a mode that belongs to the C atoms of the porphyrin ring not connected to pyrrole hydrogens. This relaxation time would only be influenced if one or the other tautomeric configuration is stabilized by interactions between the heme crevice and the macrocycle. The results show that it does not happen in the case of B_2. However, in B_3, the relaxation time becomes shorter, indicating that a stronger coupling to certain atomic groups is required to stabilize the structure of MP in this state. At the same time, the interaction is probably weaker in other directions. This result agrees with compressibility and dipole moment differences observed between the two photoproduct complexes.

(3) In the case of holes 3 and 4 the relaxation times increase from state B_1 to states B_2 and B_3, monotonically. Among typical frequencies of these holes we could identify modes which are directly connected with the reorganization of inner ring pyrrole hydrogens. This indicates why these vibrations were found to be sensitive to tautomerization.

Our results suggest that MP has tightest fit in HRP in the tautomeric state B_1, a looser fit in B_2, and the loosest in B_3. At the comparison of MP in HRP and porphin in the Xe matrix, the structure of MP in state B_1 showed the strongest resemblance to the structure of the chromophore in the Xe matrix. It can be interpreted that MP in state B_1 is distorted the least by the protein matrix. We think that these two things are in good agreement, i.e., the least distorted structure of the chromophore can most favorably be embedded by the crevice at an optimum structure of it, and this yields the tightest fit.

Acknowledgment. This work was supported by the scientific cooperative project No. 11 of Estonian and Hungarian Academies of Sciences, Estonian Science Foundation Grant No. 2314, by EC Grant ERBCIPDCT940043, by Hungarian Grants ETT 426/1996, OTKA T25545, and FKFP 1191/1997. We thank Dr. Andras Kaposi for helpful discussions and Mrs. Rozsa Markacs for technical assistance.

References and Notes

(1) Hobbs, D. J.; Shelnutt, A. J. *J. Protein Chem.* **1995**, *14*, 19.
(2) Deisenhofer, J.; Epp, O.; Miki, K.; Michel, H. H. *Nature* **1985**, *318*, 618.
(3) Angiolillo, P. J.; Leigh, J. S., Jr.; Vanderkooi, J. M. *Photochem. Photobiol*. **1982**, *36*, 133.
(4) Friedrich, J.; Scheer, H.; Zickendraht-Wendelstadt, B.; Haarer, D. *J. Chem. Phys.* **1981**, *74*, 2260.
(5) Reddy, N. R. S.; Lyle, P. A.; Small, G. J. *Photosynth. Res.* **1992**, *31*, 167.
(6) Boxer, S. G.; Gottfried, D. S.; Lockhart, D. J.; Middendorf, T. R. *J. Chem. Phys.* **1987**, *86*, 2439.
(7) Zollfrank, J.; Friedrich, J.; Vanderkooi, J. M.; Fidy, J. *J. Chem. Phys.* **1991**, *95*, 3134.
(8) Gajhede, M.; Schuller, D. J.; Henriksen, A.; Smith, A. T.; Poulos, T. L. *Nature Struct. Biol.* **1997**, *4*, 1032.
(9) Horie, T.; Vanderkooi, J. M.; Paul, K. G. *Biochemistry* **1985**, *24*, 7931.
(10) Friedrich, J.; Gafert, J.; Zollfrank, J.; Vanderkooi, J. M.; Fidy, J. *Proc. Natl. Acad. Sci. U.S.A.* **1994**, *91*, 1029.
(11) Herenyi, L.; Fidy, J.; Gafert, J.; Friedrich, J. *Biophys. J.* **1995**, *69*, 577.
(12) Voelker, S.; van der Waals, J. H. *Mol. Phys.* **1976**, *32*, 1703.
(13) Fidy, J.; Vanderkooi, J. M.; Zollfrank, J.; Friedrich, J. *Biophys. J.* **1992**, *61*, 381.
(14) Gafert, J.; Friedrich, J.; Parak, F. *J. Chem. Phys.* **1993**, *99*, 2478.
(15) Gafert, J.; Friedrich, J.; Vanderkooi, J. M.; Fidy, J. *J. Phys. Chem.* **1995**, *99*, 5223.
(16) Paul, K. G.; Stigbrand, T. *Acta Chem. Scand*. **1970**, *24*, 3607.
(17) Teale, F. W. J. *Biochim. Biophys. Acta* **1959**, *35*, 543.
(18) Avarmaa, R. A.; Rebane, K. K. *Spectrochim. Acta* **1985**, *41a*, 1365.
(19) Gafert, J.; Friedrich, J.; Vanderkooi, J. M.; Fidy, J. *J. Phys. Chem.* **1994**, *98*, 2210.
(20) Personov, R. I. In *Spectroscopy and Excitation Dynamics of Condensed Molecular Systems*; Agranovich, V. M., Hochstrasser, R. M., Eds.; North-Holland: Amsterdam, 1983; Chapter 10.
(21) Personov, R. I. *J. Photochem. Photobiol. A* **1992**, *62*, 321.
(22) Rebane, L. A.; Gorokhovskii, A. A.; Kikas, J. V. *Appl. Phys. B* **1982**, *29*, 235.
(23) Jankowiak, R.; Hayes, J. M.; Small, G. J. *Chem. Rev.* **1993**, *93*, 1471.
(24) Mauring, K. Kinetics of conversions and spectral hole burning in chlorophyll and its derivatives. Ph.D. Thesis, University of Tartu, 1982.
(25) van der Laan, H. Optical dephasing and energy transfer in disordered systems. A study by hole burning of molecules adsorbed on porous silica glass and photosynthetic complexes. Ph.D. Thesis, University of Leiden, 1992; p 69.
(26) Gorokhovskii, A. A.; Kikas, J. V. *Opt. Commun.* **1977**, *21*, 272.
(27) Kohler, B. E. In *Chemical and Biochemical Applications of Lasers*; Moore, C. B., Ed.; Academic. New York, 1979; pp 31−51.
(28) Avouris, P.; Campion, A.; El-Sayed, M. A. *J. Chem. Phys.* **1977**, *67*, 3397.
(29) Friedrich, J.; Swalen, J. D.; Haarer, D. *J. Chem. Phys.* **1980**, *73*, 705.
(30) Kaposi, A. D.; Vanderkooi, J. M. *Proc. Natl. Acad. Sci. U.S.A.* **1992**, *89*, 11371.
(31) Fidy, J.; Paul, K. G.; Vanderkooi, J. M. *Biochemistry* **1989**, *28*, 7531.
(32) Kaposi, A. D.; Fidy, J.; Stavrov, S. S.; Vanderkooi, J. M. *J. Phys. Chem.* **1993**, *97*, 6319.
(33) Radziszevsky, J. G.; Waluk, J.; Michl, J. *J. Mol. Spectrosc.* **1990**, *140*, 373.
(34) Anni, H.; Vanderkooi, J. M.; Sharp, K. A.; Yonetani, T.; Hopkins, S. C.; Herenyi, L.; Fidy, J. *Biochemistry* **1994,** *33*, 3475.
(35) Senge, M. O. *J. Photochem. Photobiol. B: Biol.* **1992,** *16*, 3.
(36) Logovinsky, V.; Kaposi, A. D.; Vanderkooi, J. M. *Biochim. Biophys. Acta* **1993**, *1161*, 149.
(37) Sapozhnikov, M. N. *Chem. Phys. Lett.* **1987**, *136*, 192.
(38) Voelker, S.; Macfarlane, R. M. *Chem. Phys. Lett.* **1979**, *61*, 421.
(39) Dicker, A. I. M.; Voelker, S. *Chem. Phys. Lett.* **1982**, *87*, 481.
(40) Solovyev, K. N.; Gladkov, L. Z.; Starukhin, A. S.; Shkirman, S. F. *Spektroskopiya porfirinov: Kolebatelnye sostoyaniya* (*Spectroscopy of Porphyrins: Vibrational States*); Nauka i Tehnika: Minsk, 1985; pp 242−243.